SPARC-RF-07/001
22 January 2007

DESIGN OF INPUT COUPLERS FOR TRAVELING WAVE STRUCTURES

D. Alesini, A. Gallo, B. Spataro *(INFN/LNF)*
A. Marinelli, L. Palumbo (*Univ. of Rome "La Sapienza"*)

Abstract

In the paper we illustrate the procedure to design couplers for traveling wave (TW) structures with 3D electromagnetic codes in frequency domain. Simple equivalent circuit models of TW structures with input and output couplers and related properties are discussed. An example of coupler design of $2\pi/3$ X band structure is illustrated.

1 INTRODUCTION

TW structures coupler design can be performed using 3D electromagnetic (e.m.) codes in frequency domain. The technique can be applied to both accelerating [1] and deflecting [2] devices. In the first paragraph of the paper we introduce a simple equivalent circuit model of TW structures with input and output couplers and we discuss some important related properties. In the second paragraph we illustrate the procedure to design couplers with 3D e.m. codes. In particular we will refer to the e.m. code HFSS [3] and we will illustrate the case of an X band $2\pi/3$ mode accelerating structure.

2 CIRCUIT MODEL OF TW STRUCTURE

The sketch of a disc loaded TW structure is shown in Fig. 1. The cells of the TW section have to be designed in order to have phase velocity of the working mode equal to the beam velocity [1]. The coupler cell dimensions have to be designed in order to minimize the reflected power at the waveguide input/output ports.
Since it is not possible to consider an infinite number of TW cells (or, equivalently, a boundary condition that perfectly matches the traveling wave with a finite number of cells), one possible strategy to design the couplers is to consider a TW structure with input and output couplers and few cells (Fig. 1). In this case it is possible to design the couplers by changing their dimensions minimizing the reflection coefficient at the waveguide input port. However, this not necessarily corresponds to a minimization of the coupler reflection coefficient. At a given frequency, in fact, one can have zero reflection coefficient at the waveguide input port because of cancellation between the reflected waves generated by the input and output couplers [4]. If this is the case, some backward wave is present in the structure, perturbing the cell-to-cell, phase advance. Therefore, one also has to verify that also the phase advance per cell in the TW structure is constant and equal to the nominal one ($2\pi/3$, as example). This procedure is, in general, very time consuming and we will not consider it in the following.
In the following of the paper we propose a different design approach based on the simple circuit model of the structure with input and output couplers shown in Fig. 2. The two port networks with scattering matrix [S] correspond to the coupling cells regions that match the input/output waveguides to the disc loaded structure. Each cell of the TW structure is modeled by a two port networks, as discussed in [5].

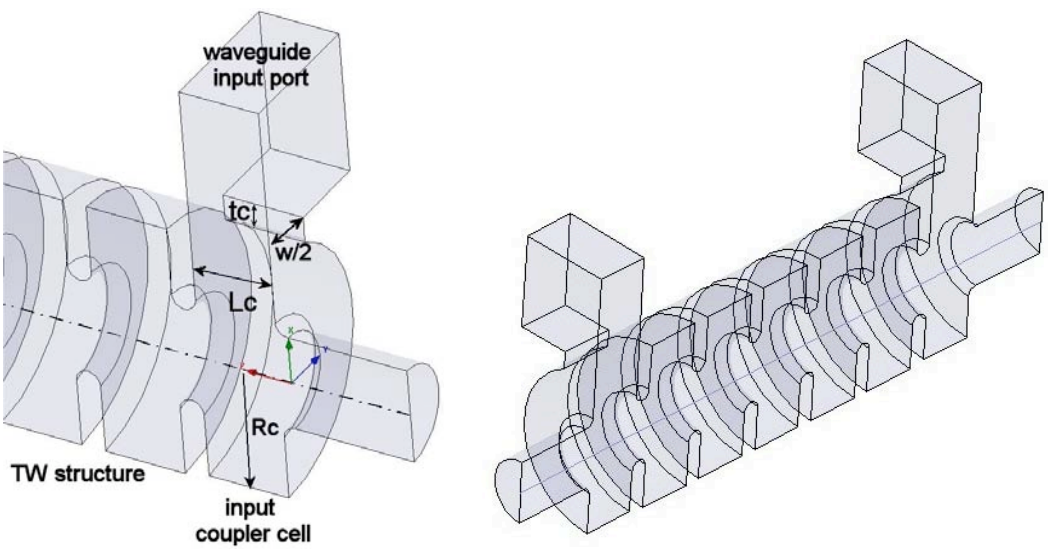

FIG. 1: sketch of a TW structure.

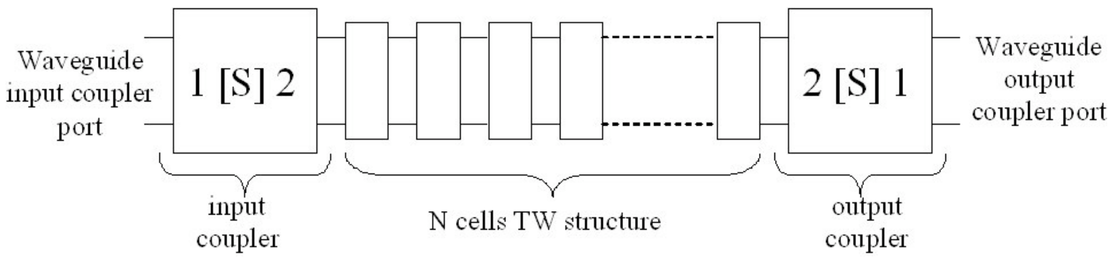

FIG. 2: equivalent circuit model of the TW structure with couplers.

From the circuit model it is easy to demonstrate the following properties.

Property 1

If we consider the short circuited structure without losses, shown in Fig. 3a whose equivalent circuit is shown in Fig. 3b, we have that (see Appendix 1):

$$S_{11} = 0 \Leftrightarrow \frac{\Gamma_s(n+2)}{\Gamma_s(n+1)} = \frac{\Gamma_s(n+1)}{\Gamma_s(n)} = e^{-j2\phi} \quad (with \quad |\Gamma_s(n)| = 1) \tag{1}$$

where $\Gamma_s(n)$ is the reflection coefficient at the coupler waveguide (n is the position of the short circuited cell), S_{11} is the first element of the coupler scattering matrix and $-\phi$ is the phase advance per cell in the TW structure.

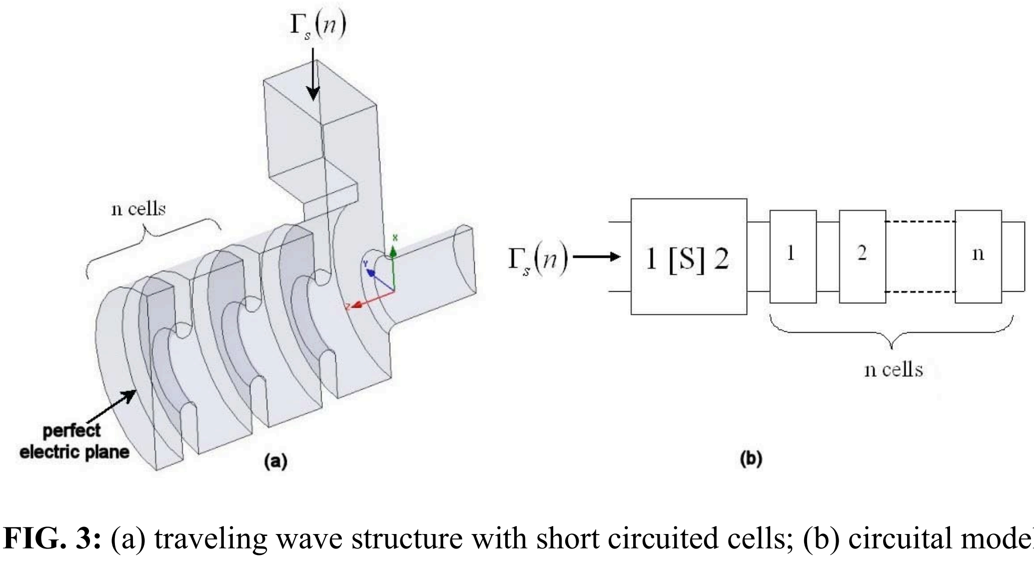

FIG. 3: (a) traveling wave structure with short circuited cells; (b) circuital model.

Property 2

Let us consider the two following quantities that represent the phase distortions at the waveguide input port due to the non ideal coupler:

$$\vartheta_{10} = \frac{\angle\left[\dfrac{\Gamma_s(n+1)}{\Gamma_s(n)}\right]}{2} + \phi$$
$$\vartheta_{21} = \frac{\angle\left[\dfrac{\Gamma_s(n+2)}{\Gamma_s(n+1)}\right]}{2} + \phi \tag{2}$$

where $\angle[x]$ indicates the phase of the complex number x. We have that (see Appendix 2):

$$|S_{11}| = \frac{1}{\sqrt{1 - 4\dfrac{\sin\phi}{\sin\vartheta_{21}}\left[\left(\cos(\phi-\vartheta_{21}) - \dfrac{\sin\phi}{\sin\vartheta_{21}}\right)\sin^2\delta_2 - \sin(\phi-\vartheta_{21})\sin\delta_2\cos\delta_2\right]}} \tag{3}$$

with:

$$\sin\delta_2 = \pm\frac{\sin(2\phi-\vartheta_{10}-\vartheta_{21})}{\sqrt{1+\dfrac{\sin^2\vartheta_{10}}{\sin^2\vartheta_{21}} - 2\dfrac{\sin\vartheta_{10}}{\sin\vartheta_{21}}\cos(2\phi-\vartheta_{10}-\vartheta_{21})}} \tag{4}$$

The procedure gives two solutions for $|S_{11}|$. As shown in Appendix 2, to select the correct solution it is necessary, first of all, to calculate the following angle:

$$\vartheta_{20}^{\ *} = 2\angle\left[1+|S_{11}|e^{j(-\eta_2+2(n+2)\phi)}\right] - 2\angle\left[1+|S_{11}|e^{j(-\eta_2+2n\phi)}\right] \tag{5}$$

where:

$$\eta_2 = \arccos\left(|S_{11}|\frac{\dfrac{1}{|S_{11}|^2} + 1 - \left(\dfrac{2\sin\phi\sin\delta_2}{\sin\vartheta_{21}}\right)^2}{2}\right) + 2\phi - \pi \tag{6}$$

The correct solution is the one that verify the following equality:

$$\vartheta_{20}^{\ *} = \vartheta_{21} + \vartheta_{10} \tag{7}$$

Property 3

From previous formulae it is easy to verify that in the "standard" cases of TW structures (with, for example, $\phi = \pi/3, 2\pi/3, 5\pi/6$), we have that:

$$\frac{\vartheta_{10}+\vartheta_{21}}{\phi} << 1 \Leftrightarrow |S_{11}| << 1 \tag{8}$$

As example the plot of $|S_{11}|$ as a function of ϑ_{10} for different values of ϑ_{21} is reported in Fig. 4 for $\phi = 2\pi/3$.
Under this condition we have that (see Appendix 3):

$$S_{11} \cong \frac{\Gamma_{c,s}(n+1) - \Gamma_{c,s}(n)e^{-j2\phi}}{1 - e^{-j2\phi}} \tag{9}$$

where $\Gamma_c(n)$ is the reflection coefficient at the input port of a complete n-cell structure (with input and output couplers) while $\Gamma_s(n)$ is the reflection coefficient of the short circuited structure of Fig. 3. In the first case n is the number of TW cells, in the other one the position of the short circuited cell.

Property 4

Under the condition (8) we have that (see Appendix 4):

$$|S_{11}| \cong \frac{1}{2(\sin\phi)^2}\sqrt{\frac{(\vartheta_{21}+\vartheta_{10})^2}{4(\cos\phi)^2} + \vartheta_{10}^2 - \vartheta_{10}(\vartheta_{21}+\vartheta_{10})} \tag{10}$$

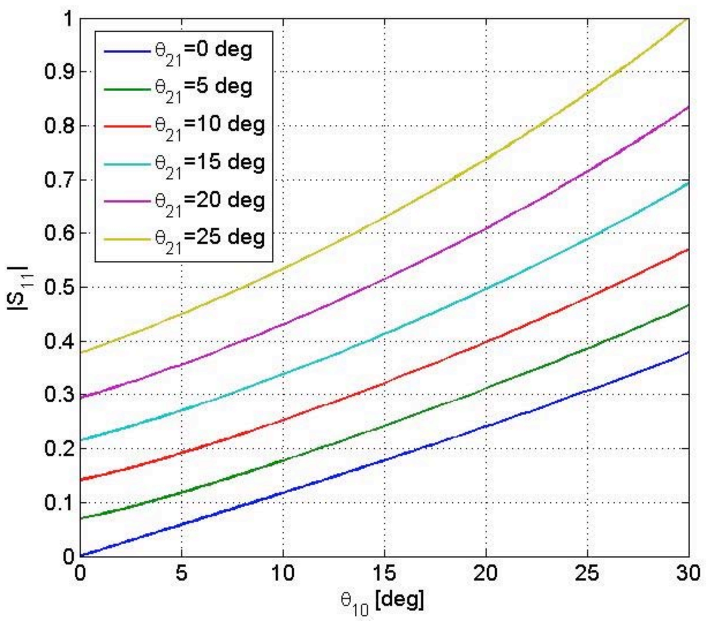

FIG. 4: $|S_{11}|$ as a function of ϑ_{10} for different values of ϑ_{21} assuming $\phi = 2\pi/3$.

3 COUPLERS DESIGN USING 3D E.M. CODES IN FREQUENCY DOMAIN

We consider, as an example, the case of a TW accelerating structure working on the $2\pi/3$ mode at 11.424 GHz. The dimensions of the single TW cell are reported in Fig. 5 and they have been found (using HFSS) in order to have the phase velocity of the fundamental harmonic equal to c at 11.424 GHz. The phase and amplitude of the longitudinal electric field on axis are reported in Fig. 6.

Considering the previous discussed properties related to the short circuited structure, it is possible to design the coupler according to the procedure discussed in detail in the following.

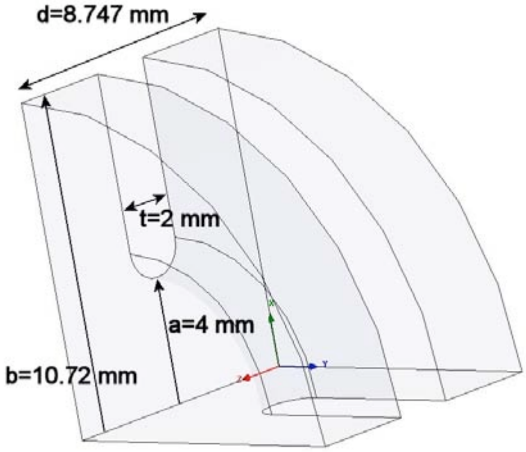

FIG. 5: TW single cell dimensions of the structure working on the $2\pi/3$ mode at 11.424 GHz.

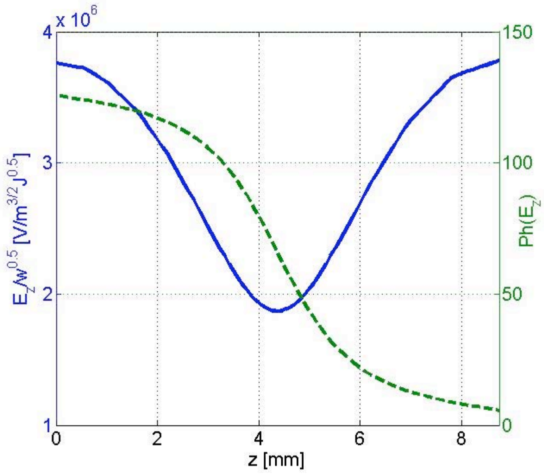

FIG. 6: phase and the amplitude of the longitudinal electric field on the axis of the single cell (HFSS results).

Let us consider the short circuited structures shown in Fig. 8 that correspond to *n=0, n=1* and *n=2* short circuited cells. The optimum coupler dimensions are those satisfying eq. (1). Starting from a non-optimized design it is possible to calculate the reflection coefficient of the coupler using (3) and change the coupler dimensions to minimize $|S_{11}|$ in a step-by-step iterative procedure. Since, as eq. (3) shows, the coupler reflection coefficient depends on the two parameters ϑ_{10} and ϑ_{21}, it is enough to vary only two of the input coupler dimensions until the residual $|S_{11}|$ value is within the specified range. Referring to the Fig. 1 sketch, simulations have shown that the most sensitive parameters are *w* and *Rc* while the length *Lc* and the thickness *tc* can be kept fixed. This procedure can be also included in an optimization algorithm to find the optimum value in a faster way as illustrated in [4].

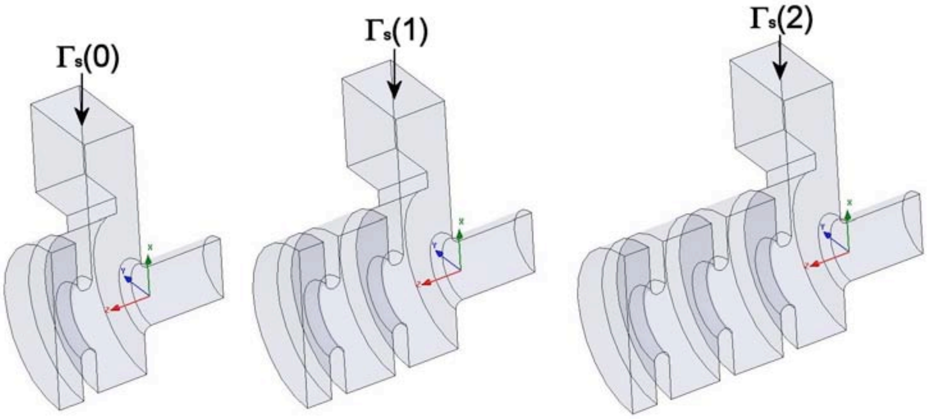

FIG. 8: short circuited structures for coupler optimization.

The values of ϑ_{10} and ϑ_{20} as functions of the geometrical parameter *Rc* near its optimum values (*Rc=10.335 mm*) are reported in Fig. 9a. The optimum value for w is 9.57 mm. The corresponding amplitudes of the reflection coefficient, calculated by eqs. (3) and (10), are reported in Fig. 9b. From this plot is easy to verify that eq. (10) can be applied only under the condition expressed by (8). Moreover from these calculations it is possible to evaluate the sensitivity of the input coupler reflection coefficient to Rc. Similar plots can be done considering the other coupler dimensions.

The amplitude of the reflection coefficient as a function of frequency, assuming the optimum values of Rc and w, is reported in Fig. 11a. It has been calculated by eq. (3) including the different single cell phase advances of the TW structure at the different frequencies given by the dispersion curve of Fig. 10. The details of the amplitude of the reflection coefficients near the working frequency 11.424 GHz calculated by eqs (3) and (10) are reported in Fig. 11b. From the plot it is easy to verify that the input coupler has reflection coefficient below 0.05 in a bandwidth of $\pm 10\,MHz$ near the working frequency. Outside this bandwidth the reflection coefficient grows and over a certain threshold eq. (10) is no more usable and we have to consider the more general expression (3).

Finally in Figs. 12 and 13 we report the simulation results of a 7 cell structure in term of electric field profiles (amplitude and phase) and reflection coefficient at the input port in the hypothesis of no losses. The finite number of reflection coefficient minima is given by the resonant SW patterns generated in the structure by the reflections at the input and output couplers. In fact, as previously observed, the coupler has a finite bandwidth and, over this, there are reflections of the traveling wave. The minima are located in the pass-band of the periodic structure shown in Fig. 10 and their number is equal to the number of cells. Increasing the number of cells we progressively increase the number of minima in the pass-band.

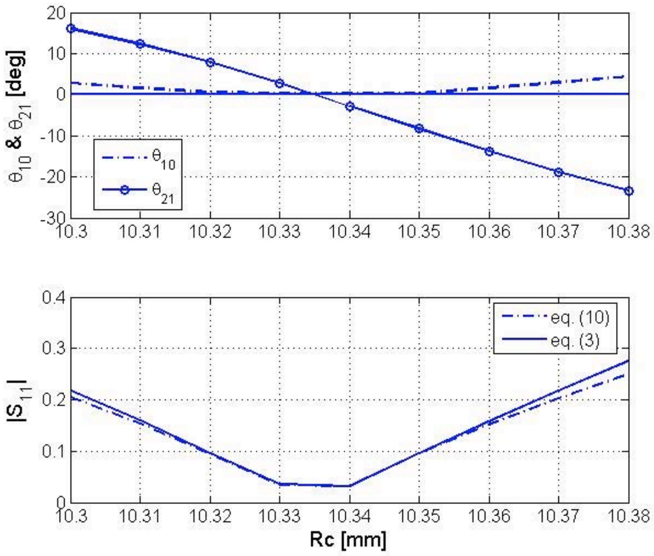

FIG. 9: (a) value of the phases $\vartheta_{10}, \vartheta_{21}$ as a function of the coupler parameters Rc (w=9.55mm); (b) amplitude of the reflection coefficient.

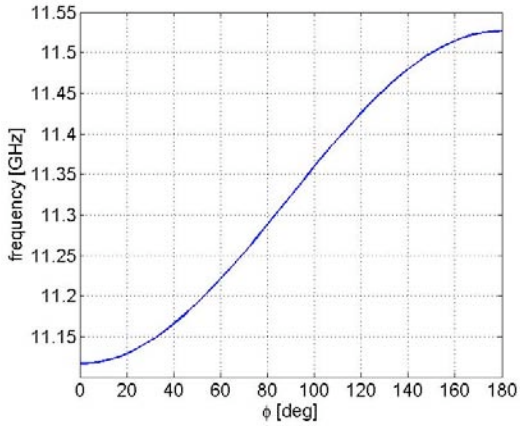

FIG. 10: TW structure dispersion curve (HFSS results).

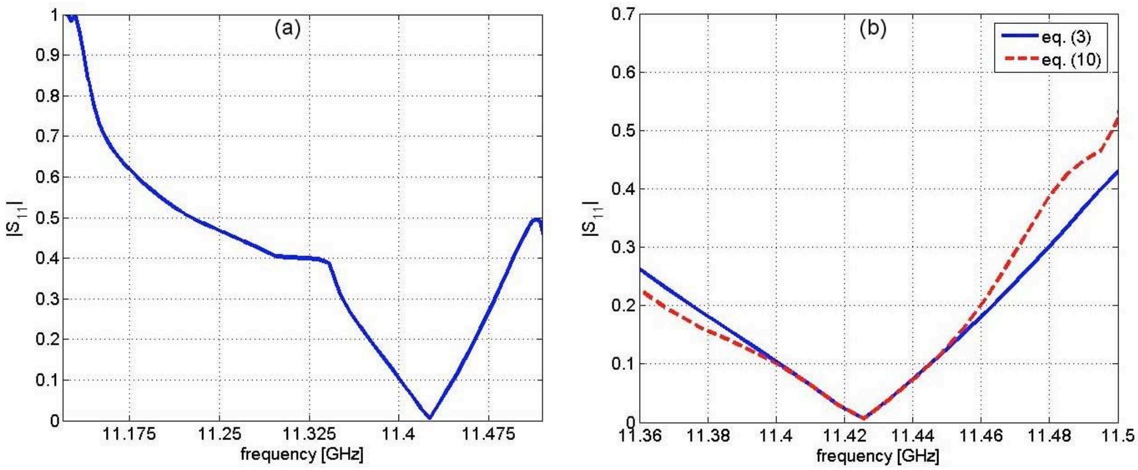

FIG. 11: amplitude of the reflection coefficient as a function of frequency.

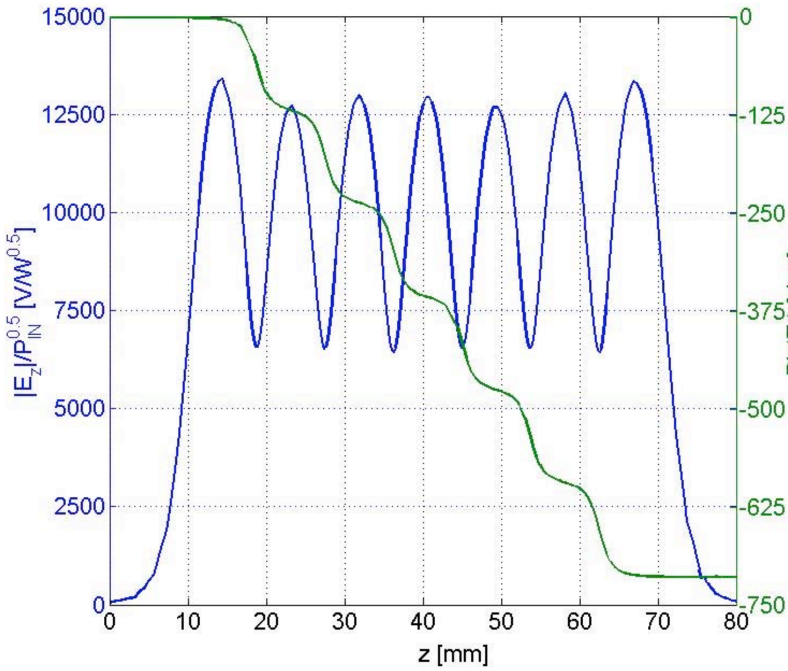

FIG. 12: Electric field on axis (amplitude and phase) as a function of the longitudinal coordinate in a 7 cell structure (HFSS results).

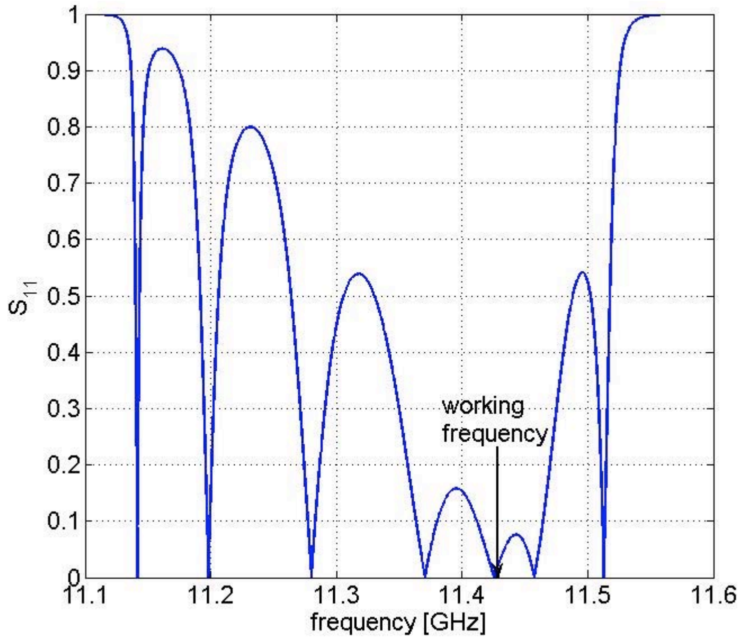

FIG. 13: Reflection coefficient at the coupler waveguide as a function of frequency in the case of a 7 cell structure (HFSS results).

This design procedure can be extended to the cases of structures with losses and/or constant gradient instead of constant impedance. In the first case the power losses in the first cells of the structure are, in general, so small [1] that it is possible to design the couplers considering the ideal structure without losses. It is easy to verify with simulations of the real structure (still considering few cells) that the results are correct. In the second case the cell dimension variations after the coupler are, in general, so small [1] that it is possible to design the couplers considering a constant impedance structure with few equal cells. In this case input and output couplers have to be designed separately to match the initial and final values of the cell irises.

4 CONCLUSIONS

We have illustrated the procedure to design couplers of TW structures with 3D electromagnetic codes working in frequency domain. The procedure is based on a proper analysis of the phase of the reflection coefficient for different length of the short circuited structures. This design procedure is based on a simple circuit model that has been presented and solved. An example of input coupler design of an X band structure, using this technique implemented with the electromagnetic code HFSS, has been finally illustrated.

5 REFERENCES

[1] P. M. Lapostolle and A. L. Septier ed., Linear Accelerators, North Holland Publishing Co., 1970.
[2] P. Bernard and H. Lengeler, On the design of disk-loaded waveguides for the RF separator. CERN 68-30, Geneva, 1968.
[3] www.ansoft.com.
[4] A. Marinelli, Tesi di Laurea, Univ. Of Rome “La Sapienza”, 2004.
[5] R.E.Collin, “Foundations for Microwave Engineering”, McGraw-Hill, Inc., 1992.

APPENDICES

Appendix 1

Let us consider the first implication:

$$S_{11} = 0 \Rightarrow \frac{\Gamma_s(n+2)}{\Gamma_s(n+1)} = \frac{\Gamma_s(n+1)}{\Gamma_s(n)} = e^{-j2\phi} \tag{1A}$$

The reflection coefficient at the input port is simply given by:

$$\Gamma_s(n) = S_{11} - \frac{S_{12}S_{21}e^{-j2n\phi}}{1+S_{22}e^{-j2n\phi}} \tag{2A}$$

If we suppose that the structure has no losses, we have that [4]:

$$\begin{cases} |S_{11}| = |S_{22}| = \alpha \\ S_{12} = S_{21} = \left(\sqrt{1-\alpha^2}\right)e^{j\eta_{12}} \\ \eta_1 + \eta_2 = 2\eta_{12} \pm \pi \end{cases} \tag{3A}$$

where α is a real number ≤ 1 and $\eta_1, \eta_2, \eta_{12}$ are the phases of the scattering coefficients S_{11}, S_{22} and S_{12} respectively.
Substituting (2A) in (1A) it follows:

$$\frac{\Gamma_s(n+2)}{\Gamma_s(n+1)} = \frac{\Gamma_s(n+1)}{\Gamma_s(n)} = e^{-j2\phi}$$

Let us now consider the other implication:

$$\frac{\Gamma_s(n+2)}{\Gamma_s(n+1)} = \frac{\Gamma_s(n+1)}{\Gamma_s(n)} = e^{-j2\phi} \Rightarrow S_{11} = 0$$

By absurd let us consider $S_{11} \neq 0$. From (2A) and (3A) we have:

$$\Gamma_s(n) = \alpha e^{j\eta_1} - \frac{\left(1-\alpha^2\right)e^{j2\eta_{12}}e^{-j2n\phi}}{1+\alpha e^{j\eta_2}e^{-j2n\phi}} = \frac{\alpha e^{j\eta_1} + e^{j(\eta_1+\eta_2-2n\phi)}}{1+\alpha e^{j\eta_2}e^{-j2n\phi}} = e^{j(\eta_1+\eta_2-2n\phi)}\frac{1+\alpha e^{j(-\eta_2+2n\phi)}}{1+\alpha e^{j(\eta_2-2n\phi)}} \tag{4A}$$

the magnitude of the reflection coefficient is always equal to 1. Concerning the phase[1] it is equal to:

$$\angle\Gamma_s(n) = \eta_1 + \eta_2 - 2n\phi + 2\angle\left[1+\alpha e^{j(-\eta_2+2n\phi)}\right] \tag{5A}$$

and therefore:

[1] The symbol $\angle[x]$ means the phase of the complex number *x*.

$$\begin{cases} \angle \dfrac{\Gamma_s(n+1)}{\Gamma_s(n)} = -2\phi + 2\angle\Big[\underbrace{1+\alpha e^{j(-\eta_2+2(n+1)\phi)}}_{c_1}\Big] - 2\angle\Big[\underbrace{1+\alpha e^{j(-\eta_2+2n\phi)}}_{c_0}\Big] \\ \angle \dfrac{\Gamma_s(n+2)}{\Gamma_s(n+1)} = -2\phi + 2\angle\Big[\underbrace{1+\alpha e^{j(-\eta_2+2(n+2)\phi)}}_{c_2}\Big] - 2\angle\Big[\underbrace{1+\alpha e^{j(-\eta_2+2(n+1)\phi)}}_{c_1}\Big] \end{cases} \tag{6A}$$

the complex numbers $c_h = 1+\alpha e^{j(-\eta_2+2(n+h)\phi)}$ can be easily plotted for h=0,1,2 and are shown in Fig. 1A. It is straightforward to verify that, except in the singular case of $\phi = \pi/2$ and $\eta_2 = 0,\pi$, the complex numbers c_0, c_1, c_2 cannot have the same phases if $\alpha \neq 0$ and therefore:

$$\frac{\Gamma_s(n+1)}{\Gamma_s(n)} \neq e^{-j2\phi} \quad \text{or} \quad \frac{\Gamma_s(n+2)}{\Gamma_s(n+1)} \neq e^{-j2\phi}$$

that is in contraddiction with the hypothesis.

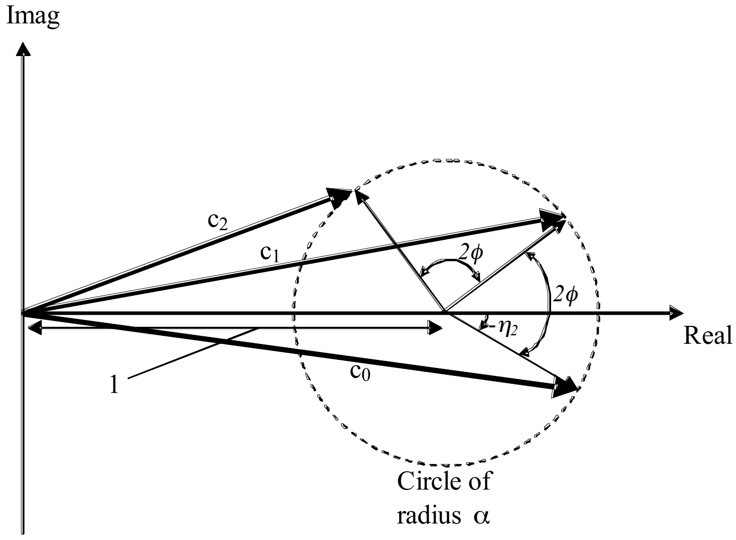

FIG 1A

Appendix 2

Figure 1A has been replotted as Fig. 2A where:

$$\vartheta_{10} = \frac{\angle\left[\dfrac{\Gamma_s(n+1)}{\Gamma_s(n)}\right]}{2} + \phi$$
$$\vartheta_{21} = \frac{\angle\left[\dfrac{\Gamma_s(n+2)}{\Gamma_s(n+1)}\right]}{2} + \phi \tag{7A}$$

By applying the sine theorem to the triangle ABO and BCO we obtain:

$$\left.\begin{aligned}\frac{\sin\vartheta_{10}}{2\alpha\sin\phi} &= \frac{\sin\delta_1}{|c_1|}\\ \frac{\sin\vartheta_{21}}{2\alpha\sin\phi} &= \frac{\sin\delta_2}{|c_1|}\end{aligned}\right\} \Rightarrow \sin\delta_1 = \frac{\sin\vartheta_{10}}{\sin\vartheta_{21}}\sin\delta_2 \tag{8A}$$

Considering the polygon ABCO we have that:

$$2\frac{\pi - 2\phi}{2} + \vartheta_{10} + \vartheta_{21} + \delta_2 + \delta_1 = 2\pi \Rightarrow \delta_1 = \pi + 2\phi - \vartheta_{10} - \vartheta_{21} - \delta_2 \tag{9A}$$

From the two equations (8A) and (9A) it is easy to derive:

$$\sin\delta_2 = \pm\frac{\sin(2\phi - \vartheta_{10} - \vartheta_{21})}{\sqrt{1 + \frac{\sin^2\vartheta_{10}}{\sin^2\vartheta_{21}} - 2\frac{\sin\vartheta_{10}}{\sin\vartheta_{21}}\cos(2\phi - \vartheta_{10} - \vartheta_{21})}} \tag{10A}$$

From the Carnot theorem applied to the triangle BOW we have:

$$1 = |c_1|^2 + \alpha^2 - 2\alpha|c_1|\cos(\phi - \vartheta_{21} - \delta_2 + \pi/2) \Rightarrow \frac{1}{\alpha^2} - 1 = \left(\frac{|c_1|}{\alpha}\right)^2 - 2\frac{|c_1|}{\alpha}\cos(\phi - \vartheta_{21} - \delta_2 + \pi/2) \tag{11A}$$

Moreover since from (8A) we have:

$$\frac{|c_1|}{\alpha} = \frac{2\sin\phi\sin\delta_2}{\sin\vartheta_{21}} \tag{12A}$$

we obtain:

$$\frac{1}{\alpha^2} - 1 = \left(\frac{2\sin\phi\sin\delta_2}{\sin\vartheta_{21}}\right)^2 - \frac{4\sin\phi\sin\delta_2}{\sin\vartheta_{21}}\cos(\phi - \vartheta_{21} - \delta_2 + \pi/2) \tag{13A}$$

From this equation it is easy to obtain eq. (3).
Concerning the choice between the two possible solutions we can apply the Carnot theorem to the triangle BOW obtaining the value of η_2 :

$$\begin{aligned}&|c_1|^2 = 1 + \alpha^2 - 2\alpha\cos(\pi + \eta_2 - 2\phi) \Rightarrow \eta_2 = \pm\arccos\left(\frac{|c_1|^2 - 1 - \alpha^2}{2\alpha}\right) + 2\phi - \pi \Rightarrow\\ &\underbrace{\Rightarrow}_{eq.(12A)} \eta_2 = \arccos\left(\alpha\frac{\frac{1}{\alpha^2} + 1 - \left(\frac{2\sin\phi\sin\delta_2}{\sin\vartheta_{21}}\right)^2}{2}\right) + 2\phi - \pi\end{aligned} \tag{14A}$$

with these values of η_2 it is possible to calculate the phase distortions at the waveguide input port due to the non ideal coupler using (6A). The correct solution for α is the one that reproduces for one of the two values of η_2 the initial phase distortions or its sum as expressed in (7).

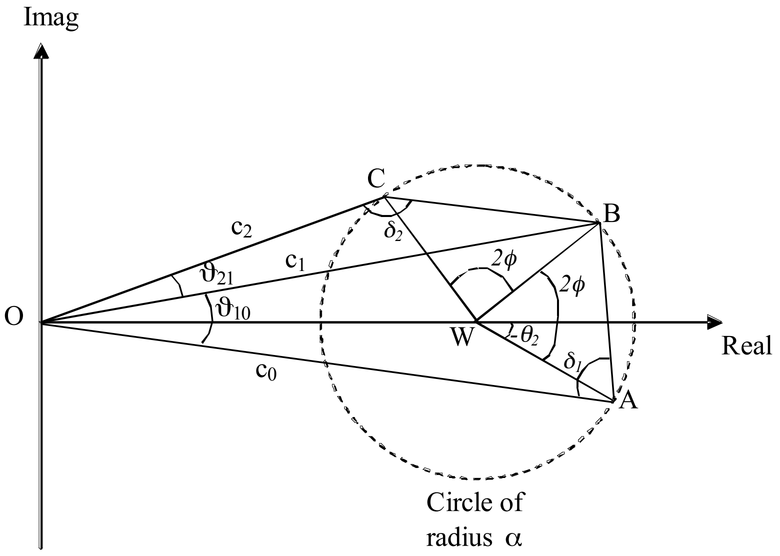

FIG 2A

Appendix 3

If $|S_{11}| << 1$ it follows from (4A) that:

$$\Gamma_s(n) = \alpha e^{j\eta_1} - \frac{\left(1-\alpha^2\right)e^{j2\eta_{12}}e^{-j2n\phi}}{1+\alpha e^{j\eta_2}e^{-j2n\phi}} \cong -e^{-j(2\eta_{12}-2n\phi)} + \alpha\left(e^{j\eta_1} + e^{j(\eta_2+2\eta_{12}-4n\phi)}\right)$$

substituting this expression in (9) we have immediately that the equality is satisfied for Γ_s.
In a similar way we have that:

$$\Gamma_c(n) = S_{11} + \frac{S_{12}^2 S_{22} e^{-j2n\phi}}{1-S_{22}^2 e^{-j2n\phi}} = \alpha e^{j\eta_1} + \frac{\left(1-\alpha^2\right)\alpha e^{j(2\eta_{12}+\eta_2-2n\phi)}}{1-\alpha^2 e^{j(2\eta_2-2n\phi)}} \cong \alpha\left[e^{j\eta_1} + e^{j(2\eta_{12}+\eta_2-2n\phi)}\right]$$

substituting this expression in (9) we have immediately that the equality is satisfied also for Γ_c.

Appendix 4

Considering the expression (5A) if $|S_{11}| = \alpha << 1$ we have:

$$\angle\Gamma_s(n) = \eta_1 + \eta_2 - 2n\phi + 2\arctan\left(\frac{\alpha\sin(2n\phi-\eta_2)}{1+\alpha\cos(2n\phi-\eta_2)}\right) \cong \eta_1 + \eta_2 - 2n\phi + 2\alpha\sin(2n\phi-\eta_2)$$

and therefore:

$$\begin{cases}\vartheta_{10} = \alpha\left[\sin\left(2(n+1)\phi-\eta_2\right)-\sin\left(2n\phi-\eta_2\right)\right] = 2\alpha\sin(\phi)\cos(\phi-\eta_2)\\ \vartheta_{20} = \vartheta_{21}+\vartheta_{10} = 2\alpha\sin(2\phi)\cos(2\phi-\eta_2)\end{cases}\Rightarrow$$

$$\frac{\vartheta_{20}}{2\alpha\sin(2\phi)} - \cos(\phi)\cos(\phi-\eta_2) = -\sin(\phi)\sin(\phi-\eta_2)\Rightarrow$$

$$\left(\frac{\vartheta_{20}}{2\alpha\sin(2\phi)}\right)^2 + \cos^2(\phi)\cos^2(\phi-\eta_2) - \frac{\vartheta_{20}\cos(\phi-\eta_2)}{2\alpha\sin(\phi)} = \sin^2(\phi)\sin^2(\phi-\eta_2)\Rightarrow$$

$$\left(\frac{\vartheta_{20}}{2\alpha\sin(2\phi)}\right)^2 + \cos^2(\phi)\left(\frac{\vartheta_{10}}{2\alpha\sin(\phi)}\right)^2 - \frac{\vartheta_{10}\vartheta_{20}}{\left[2\alpha\sin(\phi)\right]^2} = \sin^2(\phi)\left[1-\left(\frac{\vartheta_{10}}{2\alpha\sin(\phi)}\right)^2\right]\Rightarrow$$

$$\left(\frac{\vartheta_{20}}{\cos(\phi)}\right)^2 + \left[2\vartheta_{10}\cos(\phi)\right]^2 - 4\vartheta_{10}\vartheta_{20} = \sin^2(\phi)\left[16\alpha^2\sin^2(\phi) - 4\vartheta_{10}^2\right]\Rightarrow$$

$$\left(\frac{\vartheta_{20}}{\cos(\phi)}\right)^2 + 4\vartheta_{10}^2 - 4\vartheta_{10}\vartheta_{20} = 16\alpha^2\sin^4(\phi)$$

from this last equality it is easy to derive eq. (10).